Climate Dynamics (2019) 53:879–893
https://doi.org/10.1007/s00382-019-04618-2

An interdecadal change in the influence of the Central Pacific ENSO on the subsequent north tropical Atlantic spring SST variability around the mid-1980s

Xiaoxue Yin[1,2] · **Lian-Tong Zhou**[1]

Received: 8 July 2018 / Accepted: 5 January 2019 / Published online: 10 January 2019

Abstract
North tropical Atlantic (NTA) spring sea surface temperature (SST) tends to be warmer (cooler) than normal in Central Pacific (CP) El Niño decaying years during 1960s to mid-1980s. However, the relationship between the NTA spring SST and CP El Niño-Southern Oscillation (ENSO) is weakened after mid-1980s. This study presents this interdecadal change and investigates possible causes. Before the mid-1980s, above-normal NTA SST peaks in post-El Niño spring. The CP El Niño can affect NTA spring SST by inducing a negative phase of North Atlantic Oscillation (NAO) anomaly over North Atlantic from winter to spring. This negative NAO circulation weakens the Azores High and causes weaker than normal trade wind. As a result, less heat loses from the NTA Ocean and above-normal SST anomalies generated. In contrast, after the middle 1980s, the connection between CP ENSO and NAO-like anomaly has been disrupted. This leads to a weakening of CP ENSO influences on the NTA spring SST. The observed change in the relationship between NTA spring SST and CP ENSO is likely related to the state of the polar vortex. Before the middle 1980s, the polar vortex is weak, this favors the propagation of ENSO-related wave flux. The Rossby wave trains spread to the stratosphere during El Niño conditions and cause weaker than normal polar vortex, resulting in a negative NAO in the low levels. And the subtropical jet is enhanced and elongated which provides a potential waveguide for wave activity propagating to the Atlantic through a tropospheric way. However, the polar vortex is strong after mid-1980s, preventing the propagation of the ENSO-related wave trains through the stratosphere or the troposphere.

Keywords North tropical Atlantic SST · CP ENSO · Interdecadal change · NAO · Polar vortex

1 Introduction

Northern tropical Atlantic pattern is one of the several prominent modes in tropical Atlantic sea surface temperature (SST) variability (e.g., Enfield and Mayer 1997; Huang et al. 2004; Huang and Shukla 2005; Handoh et al. 2006), with SST anomalies extending westward into the Caribbean from the coast of northern Africa in seasonal to interannual timescales. Previous studies have elaborated that NTA SST anomalies have tremendous influence on climate variability in the surrounding and remote regions (e.g., Folland et al. 1986; Saravanan and Chang 2000; Cassou and Terray 2001; Cassou et al. 2004; Wu and Kirtman 2011; Wu et al. 2011; Hatzaki and Wu 2015; Zhou and Wu 2015; Chen and Wu 2017). For example, Saravanan and Chang (2000) suggested there is a "dipole" correlation structure between tropical Atlantic SST and rainfall in the Nordeste Brazil region. Hatzaki and Wu (2015) found that the winter precipitation field in south-eastern Europe is strongly correlated to the tropical North Atlantic SSTs through a Rossby wave pattern spreading from western tropical Atlantic to Europe. Furthermore, the NTA SST anomalies may also affect the Pacific ENSO (e.g., Wang et al. 2011; Ham et al. 2013, 2014; Martin et al. 2015), the generation of western North Pacific (WNP) anticyclone (e.g., Huo et al. 2015; Cao et al. 2016) and Indian monsoon (Kucharski et al. 2009). Therefore, it is of great importance to gain a better understanding of the NTA SST

✉ Lian-Tong Zhou
zlt@mail.iap.ac.cn

[1] Center for Monsoon System Research, Institute of Atmospheric Physics, Chinese Academy of Sciences, P.O. Box 2718, Beijing 100190, China

[2] College of Earth and Planetary Sciences, University of Chinese Academy of Sciences, Beijing 100049, China

variability and the influence factors in order to improve the climate prediction in the surrounding regions as well as the remote areas.

Previous studies have pointed out that the NTA SST anomalies are driven by heat flux anomalies through change in trade winds (Enfield and Mayer 1997; Carton et al. 1996; Mo and Hakkinen 2001; Czaja et al. 2002). The trade wind anomalies are associated with regional ocean–atmosphere interaction (e.g., Handoh and Bigg 2000; Wu and Liu 2002; Huang et al. 2004; Huang and Shukla 2005) as well as remote forcing, with ENSO and the North Atlantic Oscillation (NAO) being the primary drivers which account for approximately half of the NTA SST variance (Saravanan and Chang 2000; Giannini et al. 2001; Sutton et al. 2000; Huang et al. 2002; Chang et al. 2003; Liu et al. 2004; Lee et al. 2008; García-Serrano et al. 2017). The teleconnection between NTA SST and ENSO is robust, with significant positive (negative) SST anomalies in the NTA which lag about one season of El Niño (La Niña) mature phase and peak in boreal spring (MAM), as a result of reduction in the surface trade wind and decrease of latent heat losses over the region of interest (e.g., Saravanan and Chang 2000; Lee et al. 2008). Various mechanisms have been proposed to explain the connection between ENSO and NTA SST variability which involved the atmospheric bridge (Alexander et al. 2002). Most researchers explained this linkage in terms of an anomalous Walker circulation (e.g., Wang 2005) and the Rossby wave train that propagates across the Pacific-North American (PNA) region (e.g., Enfield and Mayer 1997; Giannini et al. 2000). Some others suggested a tropospheric temperature (TT) mechanism (e.g., Chiang and Sobel 2002; Chang et al. 2006) and a remote Gill-type response over the TNA region (García-Serrano et al. 2017). Previous studies suggested that the ENSO-TNA teleconnection is linear with respect to the phase of ENSO (e.g., Czaja et al. 2002; Handoh et al. 2006; Rodrigues et al. 2011; Rodrigues and McPhaden 2014). Czaja et al. (2002) found that warm El Niño years are typically associated with warm NTA conditions, and the reverse situation during La Niña years are associated with cold NTA conditions. Handoh et al. (2006) demonstrated that the composited SST anomalies of warm and cold NTA events have very similar patterns in the tropical Pacific with the opposite sign. Rodrigues et al. (2011) and Rodrigues and McPhaden (2014) further unravelled that the SSTA composited for Eastern and Central Pacific El Niño events both show warm anomalies in the NTA, and the scenario is similar for La Niña events, except that the sign of the SST anomalies is opposite.

However, previous studies confined their attention on the conventional central-eastern Pacific ENSO phenomenon (Capotondi et al. 2015), using the Niño3.4 index or the Niño3 index to describe the tropical Pacific SST variability. In fact, there also exists a Central Pacific ENSO, verified by numerous publications (Kug et al. 2009; Kao and Yu 2009; Yeh et al. 2009; Ashok et al. 2007; Weng et al. 2007), with primarily anomalous SST appears in the tropical central Pacific. Similar to the EP El Niño, the extratropical teleconnection connected to the CP El Niño events is manifested as a negative phase of NAO over North Atlantic Ocean region in boreal winter. Some studies suggested a stratospheric mechanism that connects the CP El Niño events with the NAO (e.g., Brönnimann et al. 2007). They explained that during an El Niño event, the stratospheric polar vortex is weaker than normal which favors the development of a negative phase of NAO (e.g., Perlwitz and Graf 1995). However, previous studies have contradictory results on the CP El Niño's impacts over the Northern Hemisphere (NH) polar stratosphere and NH climate. On one hand, Hegyi and Deng (2011) found a significantly stronger polar vortex during CP El Niño. On the other hand, previous studies reported an anomalously weak polar vortex in CP El Niño years in reanalysis data and two idealized simulations (Garfinkel et al. 2013; Hegyi et al. 2014). Garfinkel et al. (2013) concluded that the NH polar stratospheric response to CP El Niño is not robust, as its sign depends on the composite size, the index used, and the month or seasonal average analyzed. Calvo et al. (2017) found that CMIP5 results do not support a stratospheric pathway for a remote influence of CP ENSO events on NH teleconnections. While some others, such as Graf and Zanchettin (2012), provided a tropospheric mechanism in which the poleward propagating Rossby waves induced by anomalous heating in the tropical Pacific could be blocked by the subtropical jet and then propagate eastward to the North Atlantic region along this subtropical waveguide (e.g., Branstator 2002). Based on this, we are interested in the connection between the CP ENSO and NTA SST, by using an EMI index (Ashok et al. 2007) instead of the most used Niño3.4 index or the Niño3 index. And we find a close connection between CP ENSO and the NTA SST anomalies, which peak in the following spring after the peak of ENSO events. Another interesting phenomenon discovered in our study shows that their relationship is not stable, with an interdecadal change occurred in the mid-1980s. The nonstationary behavior of the ENSO-NAE atmospheric teleconnection has been addressed in some recent work (e.g., López-Parages et al. 2015, 2016a, b; Ayarzagüena et al. 2018). Based on the effects of El Niño on late winter European rainfall, López-Parages et al. (2015, 2016a, b) distinguished two sub-periods on the correlation between Niño 3.4 index and the principal component of the first variability mode of the Euro-Mediterranean precipitation in February–March–April (FMA). They found that the ENSO teleconnection to the NAE climate is broadly correlated over the periods 1944–1964 and 2003–2008, while they are mainly anti-correlated over the periods 1900–1940 and 1965–1984. They attributed the variable of ENSO-EuroMediterranean

rainfall link to changes in the multidecadal variability of the SST and the associated tropospheric teleconnections. Ayarzagüena et al. (2018) focused on the non-stationarity of the ENSO teleconnections to Europe through the stratosphere regardless of the type of ENSO. However, these studies mainly focus on the Euro-Mediterranean rainfall and distinguish sub-periods using a Niño 3.4 index. The teleconnections between ocean basins could be a more complicated process which may include the ocean dynamical process and the air-sea interaction process. Moreover, besides Euro-Mediterranean area, north tropical Atlantic SST anomalies could cause climate anomalies in other surrounding areas such as the intra-Americas region. Thus, the study of the interdecadal change in the relation between CP El Niño and the NTA SSTA would give rise to a hot consideration of the climate change in the surrounding areas which is related to the NTA SST or/and the CP El Niño. Therefore, we will discuss the instability of the connection between CP ENSO and NTA spring SST and the possible mechanisms.

In our study, we offer preliminary evidence of a correlation between winter CP ENSO and the following NTA spring SST. Moreover, the interdecadal change of their relationship and the possible modulators are also investigated. The arrangement of the text is as follows. Section 2 describes the data and methodology used in this study. In Sect. 3, we investigate the interdecadal change in the relation between the CP ENSO and the NTA spring SST. In Sect. 4, we contrast the regression patterns of spring SST anomalies with previous winter CP ENSO index between different periods and address relevant changes in CP ENSO-related circulation anomalies to elucidate the possible pathways in which the CP ENSO could influence the NTA SST anomalies. The plausible causes for the interdecadal change are discussed in Sect. 5. Summary and discussion are provided in Sect. 6.

2 Data and methodology

The monthly mean SST is from the NOAA Extended Reconstruction SST, version 3b (ERSST.v3b; Smith et al. 2008), with a resolution of 2.0° × 2.0°, from 1854–present. A parallel analysis has been performed using SST from Met Office Hadley Center, version 1.1 (HadISST.v1.1; Rayner et al. 2003), with a resolution of 1.0° × 1.0°, ranging from 1870 to present. The results based on HadISST.v1.1 are very similar to those based on the ERSST.v3b and thus are not shown. The sea level pressure (SLP), geopotential height and wind are from the National Centers for Environmental Prediction-National Center for Atmospheric Research (NCEP-NCAR) reanalysis (Kalnay et al. 1996), with a resolution of 2.5° × 2.5°, ranging from 1948 to present. In addition, this study employs monthly mean net surface heat fluxes including net shortwave radiation flux, net longwave radiation flux, latent heat flux, and sensible heat flux from the NCEP-NCAR reanalysis. The results are confirmed by the OAflux data, with a resolution of 2.5° × 2.5°, covering the period from 1958 to 2009. For heat flux anomalies, positive (negative) anomalies indicate that the ocean gains (gives) heat from (to) the atmosphere.

Seasonal means are constructed and the annual cycle is removed. To reduce the effect of long-term trends, a first-order polynomial (i.e., linear trend) is removed from all anomalies. And the anomalies are created by subtracting the 1959–2016 mean. The main statistical methods used are the canonical correlation analysis, the linear regression analysis and the composite analysis. A Student's t test is used to assess the statistical significance of correlation–regression patterns. As the analysis windows are as short as 21 years, the effective degrees of freedom (EDOF) are taken into account when assess the statistical significance of correlations and regressions using the method discussed in Bretherton et al. (1999):

$$N' = N \times \frac{\left[1 - r_1 r_2\right]}{\left[1 + r_1 r_2\right]}, \tag{1}$$

where N′ is the EDOF, N is the original sample size, and r_1 and r_2 are the lag 1 autocorrelation coefficients of the two time series involved. Since the lag 1 autocorrelation coefficient for the EMI index is 0.46, we have $N' = 0.62N$ assuming that $r_1 = r_2$.

Following Ashok et al. (2007), CP ENSO index is defined as $\mathrm{EMI} = [\mathrm{SSTA}]_A - 0.5[SSTA]_B - 0.5[SSTA]_C$, where the square bracket with a subscript represents the area-mean SST anomaly (SSTA) averaged over three different tropical Pacific regions including the central region (A: 165°E–140°W, 10°S–10°N), the eastern part (B: 110°W–70°W, 15°S–5°N), and the western one (C: 125°E–145°E, 10°S–20°N). The November–December–January (NDJ) EMI index is used in our study to compute the related regression maps, and for convenience we denote it as ND(−1)J. The NTA spring SST index is defined as area-averaged SST anomalies over the region 4°N–25°N and 15°W–60°W and averaged over March–April–May (MAM) in the post-ENSO year. This particular index is chosen because it captures the center action of the dominant mode of NTA SST variability (e.g., Nobre and Shukla 1996; Dommenget and Latif 2000) and is most pronounced in spring (Nobre and Shukla 1996). The strength of the polar vortex in the stratosphere is measured by a stratospheric polar-night jet index (SPJI) which is defined by the zonal-mean wind at 60°N at 30 hPa (Wei et al. 2015).

The wave activity flux (Takaya and Nakamura 2001) is used to explore the stationary Rossby wave sources

and propagation induced by the CP ENSO. It is a phase-independent flux and is parallel to the local group velocity of a stationary Rossby wave train in the Wentzel–Kramers–Brillouin (WKB) approximation. The three-dimensional flux is calculated according to the following equation:

$$R_{wa} = \frac{p}{2|U|}\begin{Bmatrix} U\left(v^{2\prime} - \psi' v'_x\right) + V\left(-u'v' + \psi' u'_x\right) \\ U\left(-u'v' + \psi' u'_x\right) + V\left(u^{2\prime} + \psi' u'_y\right) \\ \frac{f_0 R_a}{N^2 H_0}\left[U\left(v'T' - \psi' T'_x\right) + V\left(-u'T' - \psi' T'_y\right)\right] \end{Bmatrix}, \quad (2)$$

where $\mathbf{U} = (U, V)$, (u', v'), ψ', T' are the climatologic zonal and meridional wind velocity, the perturbation of geostrophic wind, stream function and air temperature. R_a, H_0, f_0, N, p are the dry air gas constant, atmosphere scale height, Coriolis parameter at 45°N, buoyancy frequency and the pressure, respectively. The subscripts x and y indicate the partial derivatives in the zonal and meridional directions, respectively.

3 The interdecadal change of the relationship

In this section, we will investigate the interdecadal change of the relationship between the ND(− 1)J CP ENSO and the NTA SST. First, we calculate the lag correlation of monthly NTA SST anomalies with respect to the ND(− 1)J EMI SST in a 21-year window (Fig. 1a). Before the mid-1980s, the prominently positive SST anomalies occur in the springtime with a correlation coefficient up to 0.7, consistent with previous studies (e.g., Saravanan and Chang 2000; Lee et al. 2008). However, this connection disappears after the mid-1980s with no significant correlation signals. Thus, it suggests that the NTA spring SST has a tight connection with CP ENSO before the mid-1980s, and this connection vanished afterwards during late-1980s and 1990s. Actually, the correlation coefficient between MAM NTA index and ND(− 1)J EMI index is only 0.43 in the long-term from 1959 to 2016, indicating a 18% variance of the NTA SST explained by the EMI SST. This is because the EMI SST and the NTA SST anomalies are of same signs during most years before mid-1980s while they indicate both same- and opposite-sign signals afterwards (Fig. 1b). Figure 1b demonstrates the NTA SST index (the continuous curve) along with years of high and low phases of CP ENSO, indicated by red and blue circles. As shown in Fig. 1b, NTA SST index tends to be positive (negative) during warm (cold) CP ENSO years in P1, while this linearity is disturbed in P2. The statistical results of the relationship are shown in Table 1 by a 0.5 standard deviation criterion. A different criterion leads to a change in the number of anomalous years

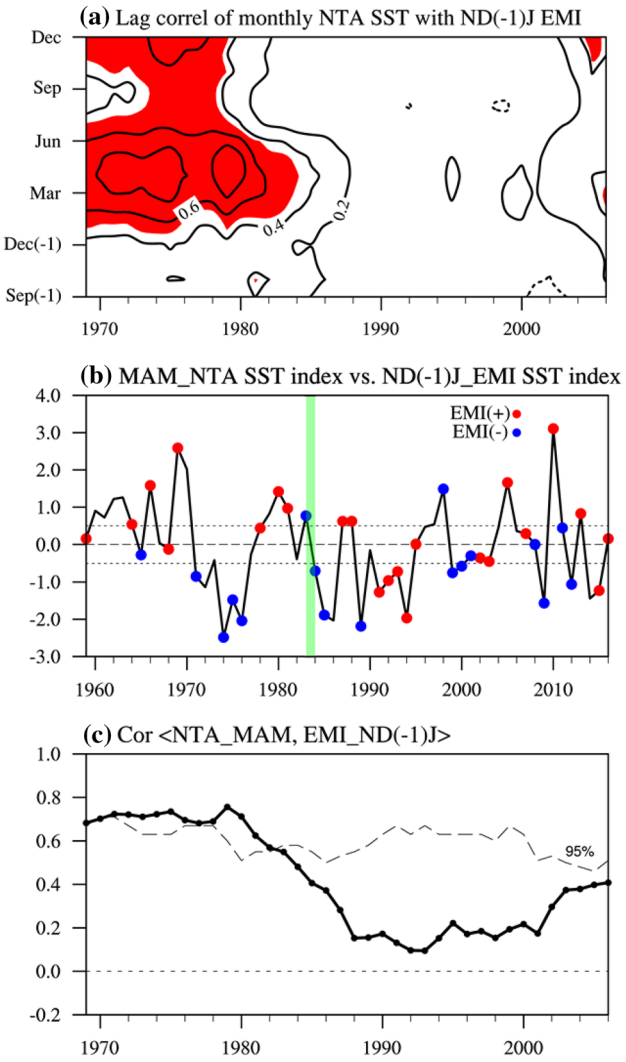

Fig. 1 **a** Lag correlation in a 21-year sliding window of monthly NTA SST (averaged over 4°N–25°N, 60°W–15°W) with respect to ND(− 1)J EMI index (red shadings represent the 95% confidence level). **b** Normalized time series of MAM NTA index (continuous curve) with years of high (larger than 0.5 SD) and low (lower than 0.5 SD) phases of CP ENSO, indicated as red and blue circles, respectively. The green line indicates the year of 1983. **c** 21-year sliding correlation of the NTA index in MAM with EMI index in ND(− 1)J (dashed line indicates the 95% confidence level). Using the ERSST.v3b datasets. And confirmed by the HadISST.v1.1 datasets

but not the statistical relationship. During 1959–1983, there are nine same-sign years and one opposite-sign year. During 1984–2016, there are twelve same-sign and six opposite-sign years. The unsteady relationship is further demonstrated by the sliding correlation between the MAM NTA SST and ND(− 1) J EMI SST with a 21-year window (Fig. 1c). The correlation is positive and significant before mid-1980s, while the connection is weak and insignificant after that. This confirms that the connection between the MAM NTA SST and ND(− 1) J EMI SST has experienced interdecadal

Table 1 Years when the MAM NTA SST and ND(− 1)J EMI SST anomalies have the same and opposite signs for 0.5 SD

	1959–1983	1984–2016
Same sign years	1964, 1966, 1969, 1971, 1974, 1975, 1976, 1980, 1981	1984, 1985, 1987,1988, 1989, 1999, 2000, 2005, 2009, 2010, 2012, 2013
Opposite sign years	1983	1991, 1992, 1993, 1994, 1998, 2015

change around the mid-1980s. The sliding correlations with different length of window, such as 17-, 19-, and 23-year are also calculated and the results show similar periods of high and low correlation.

In the following, we will select high- and low-correlation periods to further investigate the interdecadal change in winter EMI SST-spring NTA SST connection. Based on the sliding correlation in Fig. 1c and Table 1, we select one high period (1963–1983, referred to as P1) and one low-correlation period (1984–2004, referred to as P2). We select these two periods because they are not overlapping and have large contrast of the correlation. According to the Fisher's r-to-z transformation, the correlation during P2 is significantly different from that during P1 at 95% confidence level. And the correlation coefficient between the MAM NTA SST and ND(− 1) J EMI SST for P1 is 0.71, significant at 99% confidence level, while the correlation coefficient in P2 is 0.15 and insignificant.

4 Contrast of anomalous SST and circulations related to the EMI index

In this section, we contrast the regressed SST anomalies and circulation variations with respect to the ND(− 1)J EMI index between the two periods selected above to investigate the possible pathway the CP ENSO exerts its impact on the NTA spring SST and to understand why the relationship between the EMI SST and the MAM NTA SST has changed. We use the regression analysis because the ENSO-NTA teleconnection is linear with respect to the phase of ENSO, suggested by previous studies (e.g., Czaja et al. 2002). And as shown in Fig. 1b, NTA SST index tends to be positive during warm CP ENSO years and negative during cold CP ENSO years, indicating a linear connection between them. Besides, we conduct some composite analysis based on major CP El Niño events to complement the regressional analysis.

4.1 SST anomalies

Figure 2 presents SST anomalies related to the ND(− 1)J EMI index from winter to spring for the two periods. The SST anomalies are positive in the central tropical Pacific and negative in the western tropical Pacific in DJF during the two periods (Fig. 2a, e), featuring a CP El Niño pattern. This positive SST anomalies in the central tropical Pacific weakened from winter to spring, indicating a decay phase of the CP El Niño. The SST anomalies in the north tropical Atlantic are quite different for the two periods. During P1, there are significant positive SST anomalies in the north tropical Atlantic, which appear in the previous winter and peak in the spring (Fig. 2a–d). While no notable signals appear in the north tropical Atlantic for P2 (Fig. 2e–h). This confirms the strong connection between ND(− 1)J EMI SST and the MAM NTA SST anomalies during P1 and the weak connection in P2. Another notable distinction between the two periods is the SST pattern over the equatorial Pacific. The SST anomalies are more eastward shifted in P1 (Fig. 2a) compared to that in P2 (Fig. 2e). Some studies suggested that the connection between ENSO and NTA SST is related to the SST pattern over the equatorial Pacific (e.g., Taschetto et al. 2016; López-Parages et al. 2016a). But the interdecadal change of the relationship between CP ENSO and the NTA SST may not lie on the SST pattern. As shown in Fig. 2a, though the SST anomalies are more eastward shifted than that in P2 (Fig. 2e), the maximum SSTA warming for the two periods are both mainly located to the west of 150°W, which is the boundary of the Niño3 and Niño4 areas. And the SST warming extended to the eastern Pacific in P1 is not very strong and insignificant at a confidence level of 95%, thus it is probably not strong enough to affect the Atlantic basin. The reason for the interdecadal shift in the relation between CP ENSO and the NTA SST is probably related to the teleconnections which will be discussed in Sect. 5.

To complement the regressional analyses based on the EMI index, we conduct a composite analyses of SST based on major CP El Niño events in both epochs. Numbers of studies have worked on the selection of CP El Niño (e.g., Taschetto et al. 2016; Feng et al. 2017). For example, Taschetto et al. (2016) defined a warming CP El Niño event when the EMI index exceeds 1 SD threshold for at least six consecutive months. Following their results (see Table 1 in their text), there are three CP El Niño events for both period 1963–1983 (1966, 1968, and 1978) and 1984–2004 (1991, 1995, and 2003). The composited SSTA based on these major CP El Niño events in both epochs are shown in Fig. 3. In both periods, the SSTA in the central tropical Pacific show a CP El Niño-like pattern in DJF (Fig. 3a, c), which decay in the following spring (Fig. 3b, d), with a stronger amplitude in the latter period. There is a significantly positive SSTA

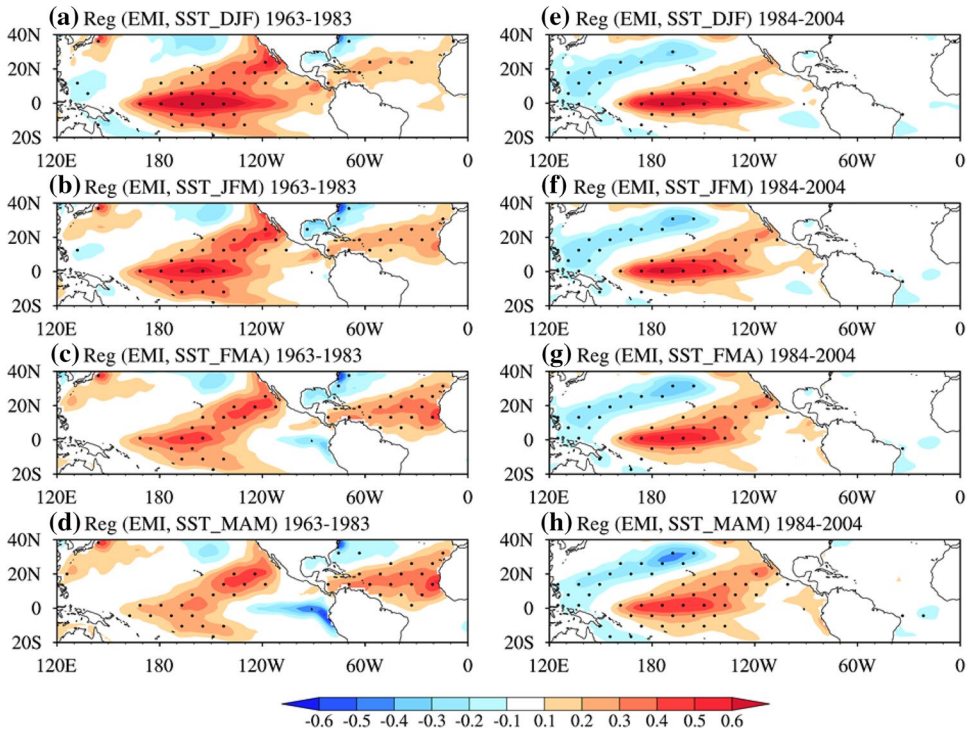

Fig. 2 Anomalous SST (units: °C; shadings) obtained by regression on the normalized ND(−1)J EMI index for **a** DJF, **b** JFM, **c** FMA, **d** MAM during 1963–1983. **e**–**h** Same as **a**–**d**, but for 1984–2004. The dotted regions indicate the 95% confidence level, based on the Student's t-test

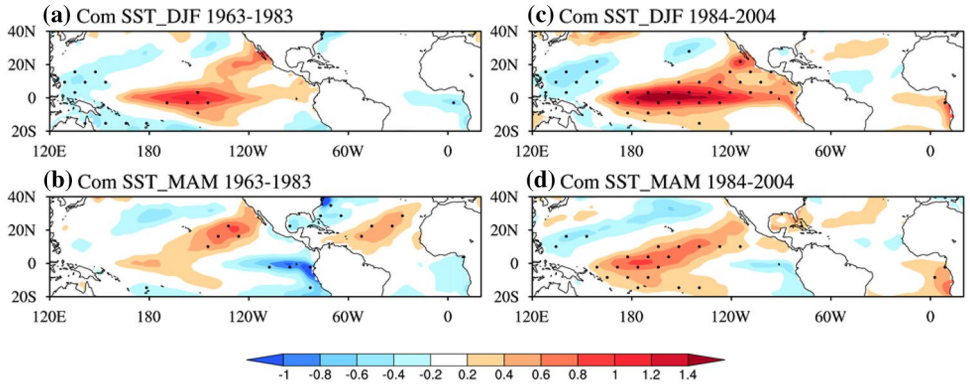

Fig. 3 Composite maps of anomalous SST (units: °C; shadings) in DJF and MAM for period 1963–1983 (**a**, **b**) and period 1984–2004 (**c**, **d**). The dotted regions indicate the 90% confidence level, based on the Student's t-test

in the north tropical Atlantic during P1 (Fig. 3b), while no notable signal occurs in P2 (Fig. 3d). These composited SSTA structures are very similar to the regression analysis with respect to the EMI index except for a larger magnitude, which further confirm the results of the interdecadal shift of the relationship between EMI SST and NTA SST.

4.2 Circulation anomalies

Figure 4 shows the regressed sea level pressure anomalies and the surface wind anomalies with respect to ND(−1)J EMI index from winter to spring for different periods. For P1, significant negative SLP anomalies are seen over the mid-latitudes and notable positive anomalies are observed over the high latitudes over North Atlantic (Fig. 4a–d). This anomalous circulation pattern resembles a negative phase of NAO. It takes place in the former winter and peaks in late winter (Fig. 4a, b). Then the NAO-like anomaly decreases and disappears in spring (Fig. 4c, d). However, in P2, there are only weak negative SLP anomalies in the high latitudes of North Atlantic, lack of a NAO-like circulation anomaly (Fig. 4e–h). This indicates that the EMI SST may influence the MAM NTA SST by generating a NAO teleconnection over North Atlantic in late boreal winter, as previous studies suggested that CP type El Niño can induce a positive NAO anomaly (e.g., Graf and Zanchettin 2012). During P1, the negative SLP anomalies in the mid-latitudes of North Atlantic in late winter could weaken the intensity of Azores High, causing anomalous southwest wind over the north tropical Atlantic area. This wind anomaly will abate the climatological northeasterly trade winds and result in less surface heat flux loss and positive SST anomalies, according to the

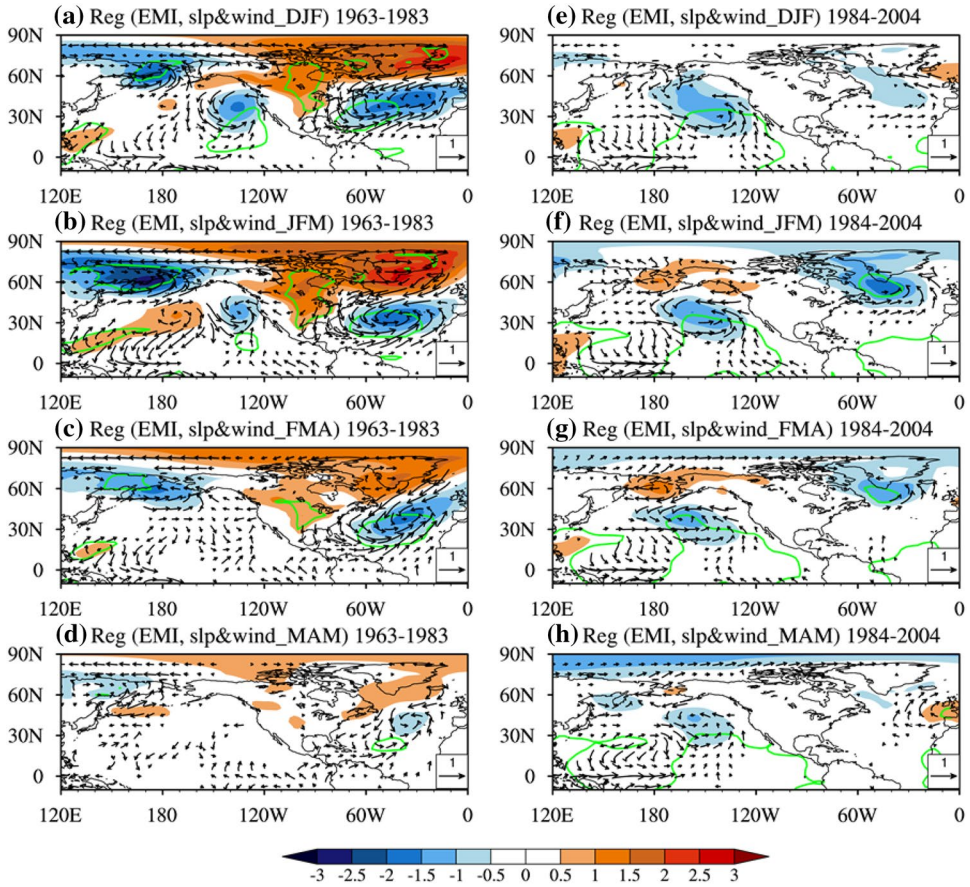

Fig. 4 Anomalies surface level pressure (units: hPa; shadings) and surface wind (units: m/s; vectors) obtained by regression on the normalized ND(− 1)J EMI index for **a** DJF, **b** JFM, **c** FMA, **d** MAM during 1963–1983. **e**–**h** Same as **a**–**d**, but for 1984–2004. The green contours indicate the 95% confidence level, based on the Student's t-test. The vectors less than 0.1 m/s are omitted

wind-evaporation-SST feedback mechanism (WES; Xie and Philander 1994). The composited results show very similar features (Fig. 5). A remarkable negative NAO-like pattern locates over the North Atlantic during P1 in winter and early spring (Fig. 5a–c). The associated surface wind fields show a southwest wind anomalies in the NTA area in the first period. This anomalous winds can reduce the climatology trade winds and give rise to the positive SSTA shown in Fig. 3b. While for P2 (Fig. 5e–g), the circulation anomalies are reversed and weaker over North Atlantic, with rather weak northeast wind anomalies in winter and southwest wind anomalies in spring. The 500 hPa height anomalies (Fig. 6) over North Atlantic are very similar to the SLP, indicating a quasi-barotropic structure.

To verify the WES mechanism, the latent heat flux anomalies (Fig. 7) regressed onto the ND(− 1)J EMI index is presented for the two periods. Surface sensible heat and radiative flux anomalies are much smaller than latent heat flux anomalies, and thus they are not shown (consistent with Klein et al. 1999). As for P1 in boreal winter (Fig. 7a), there are positive latent heat anomalies over the entire north part of the north tropical Atlantic and negative anomalies over southwest part of the north tropical Atlantic. As the anomalous southwest wind enhanced and stretched further south in late winter (Fig. 4b), the negative latent heat anomalies are weakened and the positive anomalies are strengthened and expanded (Fig. 7b). Then the heat anomalies decreased and vanished in the following seasons (Fig. 7c, d). Thus, the positive latent heat anomalies in the late winter and early spring, which indicates net heat transferred to the ocean, contribute to the generation of positive SST anomalies over north tropical Atlantic in spring. While in P2 (Fig. 7e–h), consistent with the weak circulation anomalies (Fig. 4e–h), the latent heat flux anomalies are rather weaker than that in P1.

To sum up, the key direct difference that impacts the change of the relationship between the ND(− 1)J EMI and MAM NTA SST is a NAO-like teleconnection. In the following section, we will investigate the possible mechanisms for the EMI/NAO teleconnection to gain a better understanding of the underlying physical process for the change of the relationship between the EMI SST and NTA SST.

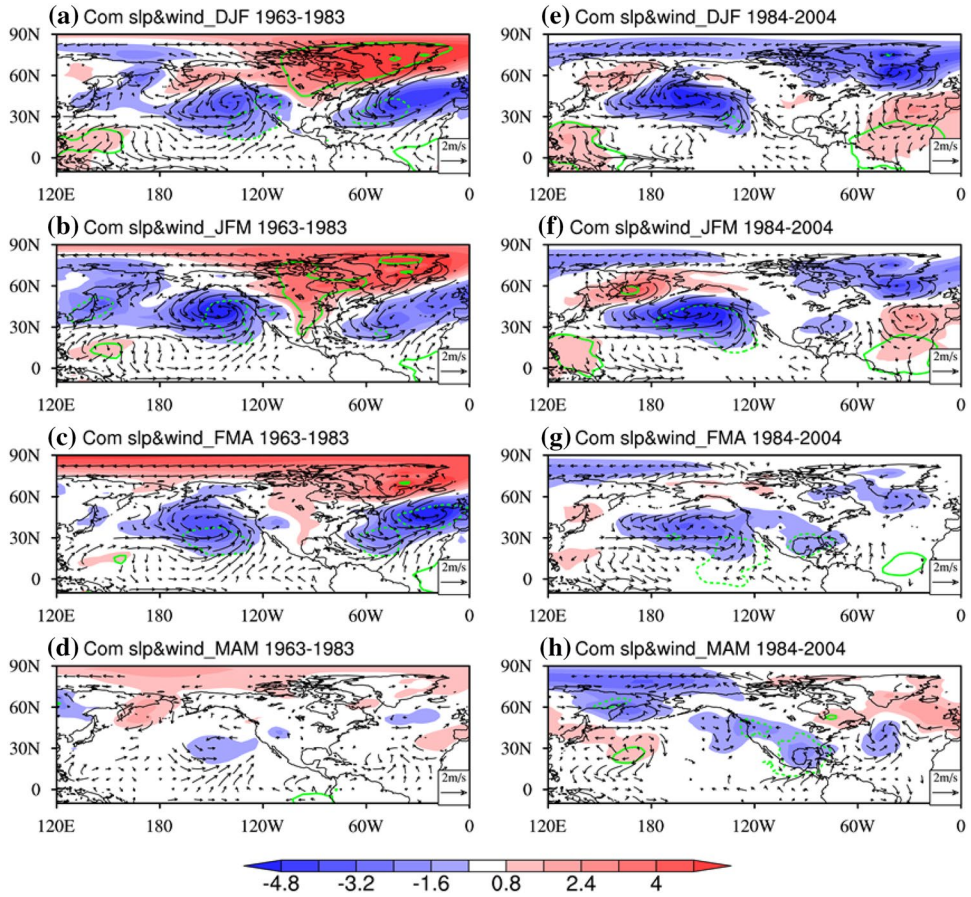

Fig. 5 Composite maps of anomalous SLP (units: hPa; shadings) and surface wind (units: m/s; vectors) for **a** DJF, **b** JFM, **c** FMA, **d** MAM during 1963–1983. **e**–**h** Same as **a**–**d**, but for 1984–2004. The green contours indicate the 95% confidence level, based on the Student's t-test. The vectors less than 0.2 m/s are omitted

5 Discussion of plausible reasons for interdecadal change in the EMI–NTA SST relationship

Why does the connection between the winter CP ENSO and the NTA spring SST differ in the two epochs? Based on the above analysis, the key link between the CP ENSO and the NTA SST is NAO anomaly which can cause surface southwest wind anomalies in the NTA region. And the results show that the EMI/NAO teleconnection is different in the two periods with close relationship in P1 and weak connection in P2. Different factors may play a role in this distinction, such as the changes in the propagations of the CP ENSO signal and the changes in location and intensity of tropical heating. Moreover, the change in the first variability mode of the atmospheric circulation over North Atlantic (NAO) may also regulate the atmospheric response to tropical Pacific heating. In this section, we first discuss the changes in the pathways of the EMI/NAO teleconnection. Then we explore the plausible factors for the interdecadal change.

To do this we will investigate the EMI-related polar vortex, subtropical westerly jet (STJ) and the wave activity flux. As mentioned in the Sect. 1, the CP El Niño/NAO teleconnection could be explained by a "stratospheric bridge" pathway as well as a "tropospheric bridge" pathway. And as suggested by previous studies, the most prominent extratropical atmosphere responses to the tropical heating anomalies mainly take place in the mid to late winter (Huang et al. 1998; Brönnimann et al. 2007), only the January–February–March (JFM) atmosphere circulation anomalies will be demonstrated in the following analysis.

5.1 The stratospheric pathway

Same as Graf and Zanchettin (2012), we use the 50 hPa height anomalies to indicate the variations of the polar vortex. Figure 8 shows the regressed geopotential height anomalies at 50 hPa with respect to the ND(− 1)J EMI SST in JFM for different periods. Previous research has documented that the stratospheric polar vortex tends to be weak during El Niño events in boreal winter (e.g., Brönnimann et al. 2007). In P1 (Fig. 8a), there are notable positive height anomalies in the whole polar region corresponding to a CP El Niño event, indicating a weaker than normal stratospheric polar vortex, consistent with previous studies. This weak polar vortex condition favors the development of a negative NAO in the surface over North Atlantic Ocean (see the SLP anomalies

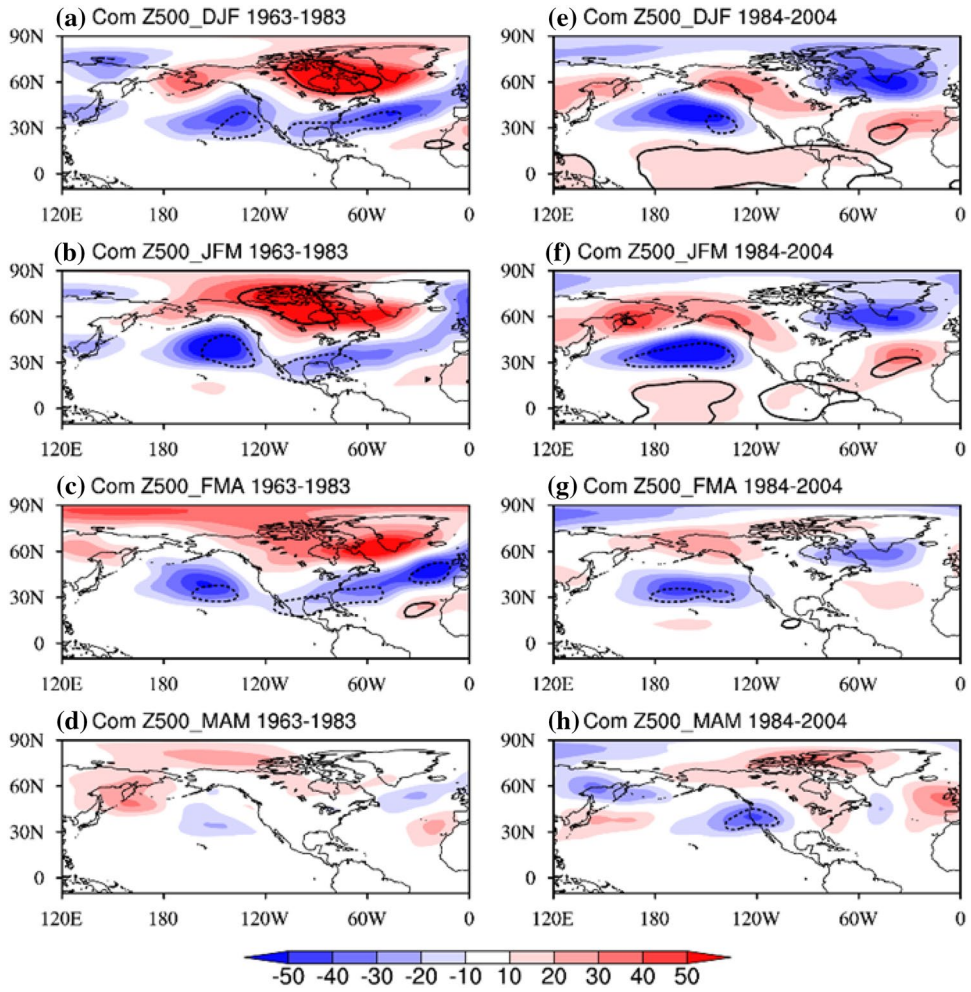

Fig. 6 Composite maps of anomalous 500 hPa geopotential height (units: m; shadings) for **a** DJF, **b** JFM, **c** FMA, **d** MAM during 1963–1983. **e**–**h** Same as **a**–**d**, but for 1984–2004. The contours indicate the 95% confidence level, based on the Student's t-test

in Fig. 4a–d; Perlwitz and Graf 1995; Chen and Wei 2009). Whereas in P2 (Fig. 8b), there is negative height anomalies in the polar cap, elucidating a reverse connection between CP El Niño and stratospheric circulation anomalies, which does not accord with previous work. The correlation coefficient between EMI index and vortex index is − 0.46 during P1, significant at 95% confidence level. This indicates that EMI SSTA can explain about 21% of vortex variance. While for P2, the correlation coefficient is only − 0.07. This certifies a closer connection between the EMI SSTA and the polar vortex in the first period than the second.

To understand the propagation of CP El Niño-related wave trains, the wave activity flux and its divergence are calculated (Fig. 9). In P1 (Fig. 9a), the divergent wave flux originated from the upper tropospheric levels near 30°N spreads poleward and propagates upward into the stratosphere at high latitudes. The convergence of the wave activity flux leads to a weakening of the zonal wind in the stratosphere through wave–mean flow interaction. Thus the polar jet stream is decelerated and the polar vortex is weakened, consistent with previous studies (e.g. Brönnimann et al. 2004; Manzini et al. 2006). In P2 (Fig. 9b), the wave activity flux derived from the upper troposphere at middle latitudes propagates horizontally to the north and refracts to the lower troposphere with almost no signal spread to the stratosphere. This contributes to the weak connection between the CP El Niño and the polar vortex.

5.2 The tropospheric pathway

Figure 10 presents the JFM 200 hPa zonal winds anomalies regressed by the ND(− 1)J EMI index in different periods. During P1, there are positive anomalies in the 200 hPa zonal winds along latitude 30°N (Fig. 10a), indicating an enhanced STJ which has a wide extension stretching from North Pacific to North Atlantic. This is consistent with previous studies who suggested that the STJ is elongated and strongly reinforced during CP El Niños due to the divergence of the meridional wave activity flux in the upper troposphere (Graf and Zanchettin 2012; Feng et al. 2017). This strengthened STJ could influence the propagation of the Rossby wave originating from the tropical Pacific and

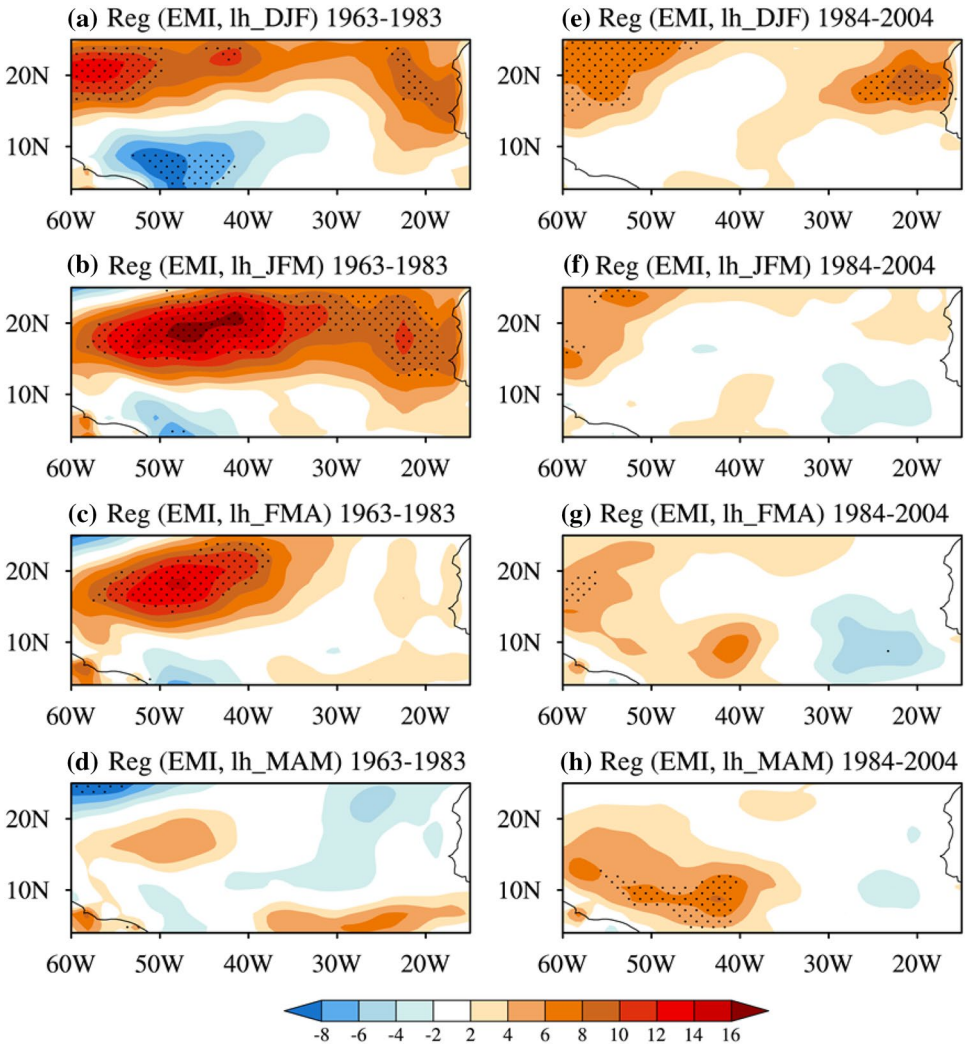

Fig. 7 Anomalies surface latent heat flux (units: W/m^2; shadings) obtained by regression on the normalized ND(− 1)J EMI index for **a** DJF, **b** JFM, **c** FMA, **d** MAM during 1963–1983. **e**–**h** Same as **a**–**d**, but for 1984–2004. The dotted regions indicate the 95% confidence level, based on the Student's t-test

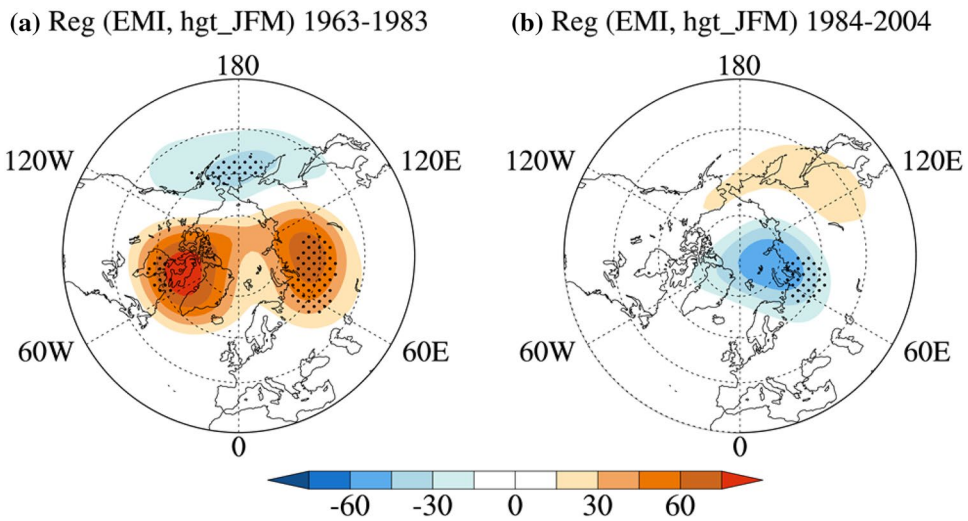

Fig. 8 Northern Hemisphere 50 hPa geopotential height anomalies (units: m) in JFM obtained by regression on the normalized ND(− 1)J EMI for **a** 1963–1983 and **b** 1984–2004. The dotted regions indicate the 90% confidence level, based on the Student's t-test

contribute to atmospheric anomalies by providing a zonal waveguide. In that case, the wave ray trajectory could be captured in the subtropical westerly jet and then propagate to the north tropical Atlantic area. To examine the propagation of the Rossby waves, the 200 hPa Rossby wave activity flux is given in Fig. 11. During P1, two branches of the

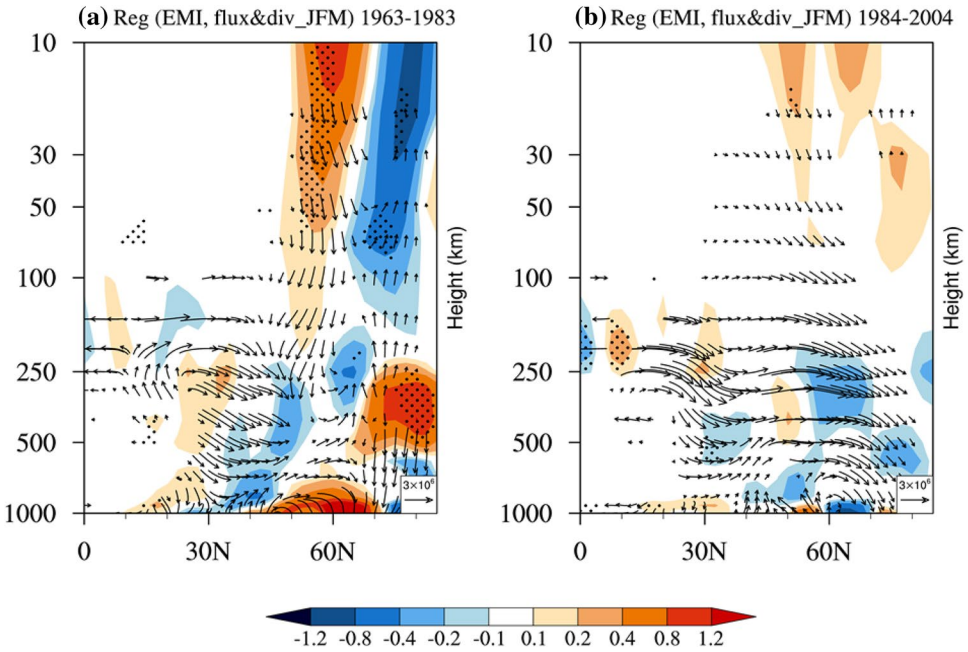

Fig. 9 Vertical wave activity flux ($\times\rho^{-1}$) (units: kg s^{-2}; vectors) and its divergence (units: m s^{-1} d^{-1}; shadings) anomalies in JFM obtained by regression on the normalized ND(− 1)J EMI for **a** 1963–1983 and **b** 1984–2004. The dotted regions indicate the 95% confidence level, based on the Student's t-test. Vectors only depict the parts exceeding 3×10^5 kg s^{-2}

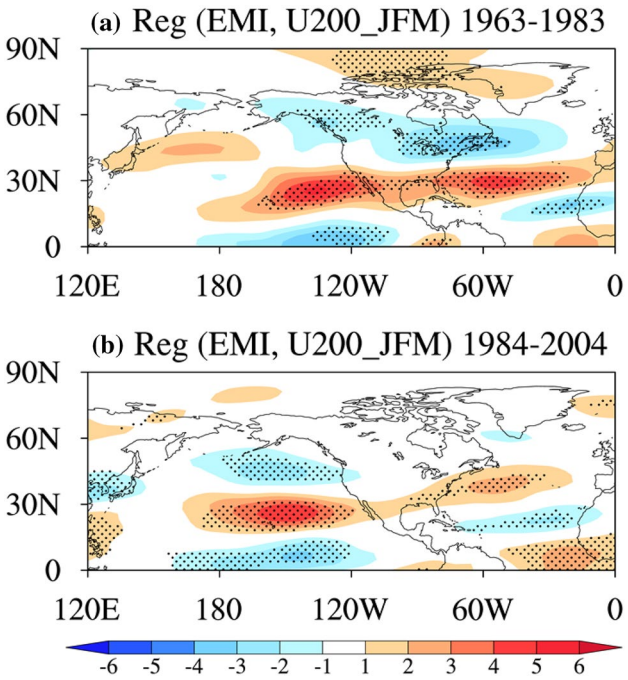

Fig. 10 Northern Hemisphere 200 hPa zonal wind (units: m/s) anomalies in JFM obtained by regression on the normalized ND(− 1)J EMI for **a** 1963–1983 and **b** 1984–2004. The dotted regions indicate the 95% confidence level, based on the Student's t-test

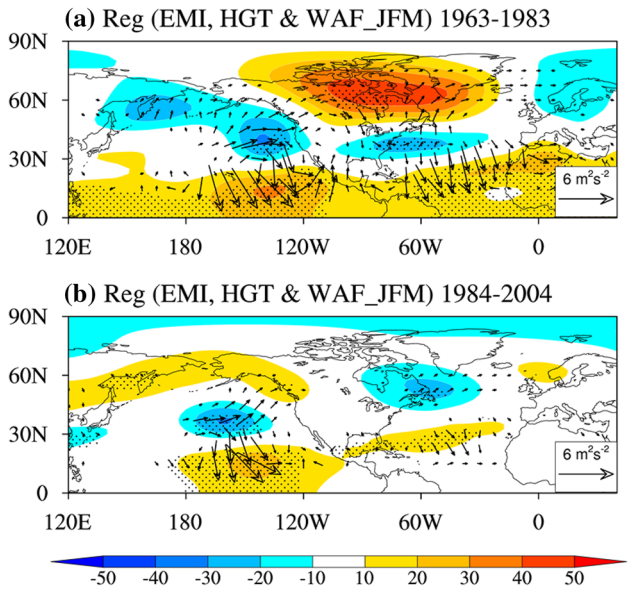

Fig. 11 200 hPa horizontal wave activity flux (units: m^2 s^{-2}; vectors) and geopotential height (units: m; shadings) anomalies obtained by regression onto the normalized ND(− 1)J EMI for **a** 1963–1983 and **b** 1984–2004. The dotted regions indicate the 95% confidence level, based on the Student's t-test. Vectors only depict the part exceeding 0.3 m^2 s^{-2}

Rossby wave activity flux originating from the North Pacific are found (Fig. 11a, vectors). The main one is equatorward which reflects at the latitudes where the zonal winds equal zero and penetrates into the North Atlantic, contributing to the negative geopotential height anomalies there in the mid-latitudes of North Atlantic (Fig. 11a, shadings). This is consistent with Jimenez-Esteve and Domeisen (2018) who suggested that downstream propagation of wave activity is increased to the North Atlantic during El Niño conditions. The other branch is northeastward with weaker strength and similar to the PNA-like pattern but shifts further east. The height anomalies at 200 hPa is similar to that in the sea

surface level (Fig. 4a–d), with positive anomalies at high latitudes and negative anomalies at mid-latitudes of Atlantic, indicating a quasi-barotropic structure. While in P2 (Fig. 10b), the enhanced zonal wind at 200 hPa is limited to the North Pacific, and the intensity is weaker compared to that in P1. The propagation of the wave activity flux in P2 (Fig. 11b, vectors) is quite different from that in P1. The equatorward branch submerged with no transfer to the North Atlantic region due to the weak and discrete zonal wind anomalies at 200 hPa (Fig. 10b). The northeast one is very weak and could not reach the Atlantic region, corresponding to the weak geopotential height anomalies in North Atlantic (Fig. 11b, shadings).

Based on the above analysis we can conclude that, in P1 the CP El Niño can enhance the STJ through the divergence of the meridional component of the Rossby wave flux, and the enhanced STJ could behave as a zonal waveguide in which the northward Rossby wave is trapped and finally propagate to the Atlantic area. However in P2, the STJ is slightly enhanced and confined to the North Pacific, thus the Rossby wave activity flux could not reach the Atlantic region.

Therefore, there are two possible pathways that the ND(−1)J EMI SST can induce a NAO anomaly pattern in boreal winter over North Atlantic and finally cause SST anomalies in the north tropical Atlantic in MAM during P1. One is a stratospheric teleconnection, the weaker polar vortex during a CP El Niño event is favorable for a negative NAO to develop. Another is a tropospheric way, the enhanced subtropical jet spreading from the Pacific Ocean to the Atlantic Ocean could provide a zonal waveguide so the Rossby wave flux originated from the Pacific could propagate eastward to the North Atlantic and cause anomalous height anomalies there. The NAO anomaly circulation will then affect NTA SST in the following spring by affecting the strength of the trade winds. However, the CP ENSO/NAO teleconnection is interrupted in P2, and there is no SST anomalies appear in spring in north tropical Atlantic. In the following section we will give a discussion on the possible factors that may impact the interdecadal change in the EMI-NTA SST relationship.

5.3 The possible factors that influence the propagation of the El Niño signal

Jimenez-Esteve and Domeisen (2018) suggested that the El Niño/NAO connection is modulated by the strength of the polar vortex by a composite analysis. They investigated the polar vortex impacts by dividing the El Niño events into strong, weak and neutral polar vortex winters. And they found that when the polar vortex is weak, the negative NAO is clear and significant in El Niño winters. This is because the weak polar vortex conditions favor the upward propagation of the Rossby wave train into the stratosphere (Charney and Drazin 1961; García-Herrera et al. 2006) and the convergence of the wave activity flux further weakens the polar vortex by reducing the polar jet, resulting in a good connection between the El Niño and the stratosphere. However, when the polar vortex is strong, the El Niño-related Rossby wave can hardly propagate to the stratosphere and polar vortex remains strong.

Here we investigate the change of the stratosphere state by using a polar vortex index. The JFM polar vortex has increased after the middle 1980s (Fig. 12), consistent with previous studies (Wei et al. 2015). Therefore, according to Jimenez-Esteve and Domeisen's results, the strong polar vortex in P2 can prevent the El Niño-related Rossby wave from propagating to the stratosphere (as shown in Fig. 9b). The polar vortex index is defined by the zonal-mean wind at 60°N at 30 hPa (Wei et al. 2015).

6 Summary and discussion

In this study, we have investigated the interdecadal change of the relationship between the winter equatorial central Pacific SST and the following NTA spring SST. The results show that the NTA spring SST has a close connection with the preceding equatorial central Pacific SST before the mid-1980s. However, the connection between the CP SST and NTA SST is weak after the mid-1980s.

Consistent changes are disclosed in the winter-to-spring circulation anomaly over North Atlantic in the decaying phase of CP El Niño. In 1963–1983, there is a pronounced negative NAO pattern developed from the preceding winter and continued to the following early spring over the North Atlantic. This EMI-related circulation anomaly weakens the climatic northeast trades wind in the subtropical North Atlantic and cause anomalous southwest winds which in turn reduce the ocean evaporation and decrease the latent heat loss. As a result, positive NTA SST anomalies take place and peak in spring. In 1984–2004, there is negative anomalies over high latitudes of North Atlantic and no notable

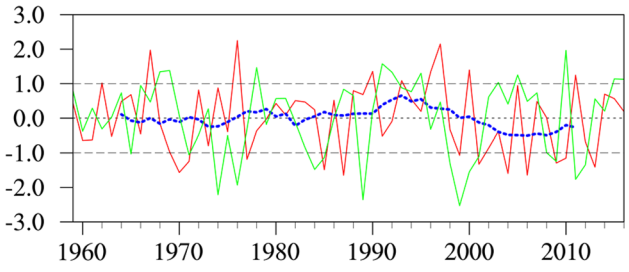

Fig. 12 The time series of the polar vortex index (red line) and EMI index (green line) for 1959–2016. The blue dashed line indicates the 11-year running average of polar vortex index

anomalies over middle latitudes. The wind and the latent heat flux anomalies are rather weak in north tropical Atlantic. This indicates a weak connection between CP El Niño and the NAO pattern.

One factor contributed to the contrasting connection between the CP ENSO and NAO circulation before and after mid-1980s is the change in the relation between the CP ENSO and the anomalous polar vortex. In 1963–1983, the CP El Niño-related polar vortex is weakened in the late winter. This is favorable for the development of a negative NAO anomaly. In 1984–2004, the CP El Niño-related polar vortex is enhanced. The change of the connection between the CP ENSO and the polar vortex may relate to the enhanced polar vortex after the mid-1980s. The enhanced polar vortex prevents the wave flux from propagating to the stratospheric levels.

Another cause for the change of the relationship between the CP ENSO and NAO circulation is the anomalous STJ. Before mid-1980s, the CP El Niño-related STJ reinforced and lengthened. It provides a zonal waveguide for the transient wave to spread to the downstream. This will finally give rise to the formation of a NAO anomaly. However in 1984–2004, the STJ is confined to the North Pacific and the wave train could not reach the North Atlantic area. Besides, previous studies (Butler et al. 2014; Jimenez-Esteve and Domeisen 2018) suggested that the strength of polar vortex play a key role in the propagation of the El Niño signs. They argued that the eastward propagation will decrease when the polar vortex is strong. As we mentioned above, the polar vortex is weak before mid-1980s and enhanced afterward. Thus the strengthening of the polar vortex strength after the mid-1980s may disrupt the propagation of the El Niño-related wave trains through the tropospheric pathway.

In the current study, we discovered that the CP ENSO can influence the NTA spring SST anomalies through inducing a NAO anomaly, indicating a potential predictability of spring NTA by tropical central Pacific SST. However, this connection may vary with time periods according to the state of the polar vortex. Therefore, the phase of the polar vortex should be taken into account in the ENSO based prediction of NTA spring SST. And as the ENSO-NTA SST connection changes, the NTA SST-related climate anomalies over surrounding areas may vary among different periods.

As mentioned in the Sect. 1, some studies argued that the NTA warming caused by El Niño events can be partially explained via the tropical-wide TT mechanism (e.g., Chiang and Sobel 2002) and the Walker circulation (e.g., Wang 2005). We inspect these two mechanisms by conducting regression analyses of some variables (e.g., TT, total cloud cover and vertical circulation) with respect to the EMI index (not shown). The results show that though the tropospheric warming can transport to the downstream to the Atlantic area in period one (while in the second period the tropospheric warming is confined to the tropical Pacific), it could not be the main factor for the SST warming in NTA due to the small radiative forcing compared to the latent heat flux anomalies caused by surface wind anomalies. The vertical circulation anomalies demonstrate that the descending motions in the tropical Atlantic have almost the same strength in the two echoes. Therefore it suggests that these factors may not be the main reasons for the interdecadal change between NTA SST and EMI SST.

In fact, the SST variability in the NTA region is quite complicated. Previous studies have addressed that the NTA SST variability is related to ENSO and extratropical atmospheric disturbance, such as the NAO (e.g., Huang and Shukla 2005; Marshall et al. 2001). And the NTA SST variability can interact with the NAO which also has interdecadal changes (Chen et al. 2015). More work is needed to understand the separate roles of ENSO and atmospheric perturbation in the development of the NTA SST anomalies. Another issue to be addressed for future study is the relative contribution of the two pathways through which the CP ENSO could cause a NAO anomaly. Furthermore, it would also be interesting to analyze either the CMIP5 simulations or sensitivity experiments to verify the conclusions presented here. We've done some simple analysis on the CMIP5 simulations and the results show that a few models could simulate the influence of CP ENSO on the NTA SST. But the CMIP5 simulations show weak skill in simulating the interdecadal change between the two series. The possible mechanism for the different simulation abilities among models and the weak skill in simulating the interdecadal shift will be investigated in the future.

Acknowledgements This paper was supported by the National Key Research and Development Program of China (Grant no. 2016YFA0600603), the National Natural Science Foundation of China (Grant no. 41475053).

References

Alexander MA, Blade I, Nerman M, Lanzante JR, Lau NC, Scott JD (2002) The atmospheric bridge: the influence of ENSO teleconnections on air–sea interaction over the global oceans. J Clim 15:2205–2231

Ashok K, Behera SK, Rao SA, Weng H, Yamagata T (2007) El Niño Modoki and its possible teleconnection. J Geophys Res 112:C11007. https://doi.org/10.1029/2006JC003798

Ayarzagüena B, López-Parages J, Iza M, Calvo N, Rodríguez-Fonseca B (2018) Stratospheric role in interdecadal changes of El Niño impacts over Europe. Clim Dyn. https://doi.org/10.1007/s00382-018-4186-3

Branstator G (2002) Circumglobal teleconnections, the jet stream waveguide, and the North Atlantic oscillation. J Clim 15:1893–1910

Bretherton CS, Widmann M, Dymnikov VP, Wallace JM, Blad I (1999) The effective number of spatial degrees of freedom of a time-varying field. J Clim 12:1990–2009

Brönnimann S, Luterbacher J, Staehelin J, Svendby TM, Hansen G, Svenøe T (2004) Extreme climate of the global troposphere and stratosphere 1940–1942 related to El Niño. Nature 431:971–974

Brönnimann S, Xoplaki E, Casty C, Pauling A, Luterbacher J (2007) ENSO influence on Europe during the last centuries. Clim Dyn 28:181–197. https://doi.org/10.1007/s00382-006-0175-z

Butler AH, Polvani LM, Deser C (2014) Separating the stratospheric and tropospheric pathways of El Niño Southern Oscillation teleconnections. Environ Res Lett 9(2):024014. https://doi.org/10.1088/1748-9326/9/2/024014

Calvo N, Iza M, Hurwitz M, Manzini E, Peña-Ortiz C, Butler A, Cagnazzo C, Ineson S, Garfinkel C (2017) Northern Hemisphere stratospheric pathway of different El Niño flavors in stratosphere-resolving CMIP5 models. J Clim 30:4351–4371

Cao X, Chen SF, Chen GH, Wu RG (2016) Intensified impact of northern tropical Atlantic SST on tropical cyclogenesis frequency over the western North Pacific after the late 1980s. Adv Atmos Sci 33:919–930. https://doi.org/10.1007/s00376-016-5206-z

Capotondi A et al (2015) Understanding ENSO diversity. Bull Am Meteor Soc 96:921–938. https://doi.org/10.1175/BAMS-D-13-00117.1

Carton JA, Cao XH, Giese BS, daSilva AM (1996) Decadal and interannual SST variability in the tropical Atlantic Ocean. J Phys Oceanogr 26:1165–1175

Cassou C, Terray L (2001) Dual influence of Atlantic and Pacific SST anomalies on the North Atlantic/Europe winter climate. Geophys Res Lett 28:3195–3198. https://doi.org/10.1029/2000GL012510

Cassou C, Deser C, Terray L, Hurrell JW, Drevillon M (2004) Summer sea surface temperature conditions in the North Atlantic and their impact upon the atmospheric circulation in early winter. J Clim 17: 3349–3363. https://doi.org/10.1175/1520-0442(2004)017,3349:SSSTCI.2.0.CO;2

Chang P, Saravanan R, Ji L (2003) Tropical Atlantic seasonal predictability: the roles of El Niño remote influence and thermodynamic air-sea feedback. Geophys Res Lett 30:1501. https://doi.org/10.10029/2002GL016119

Chang P, Fang Y, Saravanan R, Ji L, Seidel H (2006) The cause of the fragile relationship between the Pacific El Niño and the Atlantic Niño. Nature 443:324–328. https://doi.org/10.1038/nature05053

Charney JG, Drazin PG (1961) Propagation of planetary-scale disturbances from the lower into the upper atmosphere. J Geophys Res 66:83–109

Chen W, Wei K (2009) Anomalous propagation of the quasi-stationary planetary waves in the atmosphere and its roles in the impact of the stratosphere on the East Asian winter climate. Adv Earth Sci 24(3):272–285. https://doi.org/10.3321/j.issn:1001-8166.2009.03.006 **(in Chinese)**

Chen SF, Wu RG (2017) Interdecadal changes in the relationship between interannual variations of spring North Atlantic SST and Eurasian surface air temperature. J Clim 30:3771–3787. https://doi.org/10.1175/JCLI-D-16-0477.1

Chen SF, Wu RG, Chen W (2015) The changing relationship between interannual variations of the North Atlantic Oscillation and Northern Tropical Atlantic SST. J Clim 28:485–504. https://doi.org/10.1175/JCLI-D-14-00422.1

Chiang JCH, Sobel AH (2002) Tropical tropospheric temperature variations caused by ENSO and their influence on the remote tropical climate. J Clim 15:2616–2631. https://doi.org/10.1175/1520-0442(2002)015,2616:TTTVCB.2.0.CO;2

Czaja A, Van der Vaart P, Marshall J (2002) A diagnostic study of the role of remote forcing in tropical Atlantic variability. J Clim 15:3280–3290

Dommenget D, Latif M (2000) Interannual to decadal variability in the tropical Atlantic. J Clim 13:777–792

Enfield DB, Mayer DA (1997) Tropical Atlantic sea surface temperature variability and its relation to El Niño-Southern Oscillation. J Geophys Res 102(C1):929–945. https://doi.org/10.1029/96JC03296

Feng J, Chen W, Li YJ (2017) Asymmetry of the winter extra–tropical teleconnections in the Northern Hemisphere associated with two types of ENSO. Clim Dyn 48:2135–2151. https://doi.org/10.1007/s00382-016-3196-2

Folland C, Palmer T, Parker D (1986) Sahel rainfall and worldwide sea temperatures 1901–85. Nature 320:602–607. https://doi.org/10.1038/320602a0

García-Herrera R, Calvo N, Garcia RR, Giorgetta MA (2006) Propagation of ENSO temperature signals into the middle atmosphere: a comparison of two general circulation models and ERA-40 reanalysis data. J Geophys Res 111:D06101. https://doi.org/10.1029/2005JD006061

García-Serrano J, Cassou C, Douville H, Giannini A, Doblas-Reyes FJ (2017) Revisiting the ENSO teleconnection to the tropical North Atlantic. J Clim 30:6945–6957. https://doi.org/10.1175/JCLI-D-16-0641.1

Garfinkel CI, Hurwitz MM, Waugh DW, Butler AH (2013) Are the teleconnections of central Pacific and eastern Pacific El Niño distinct in boreal wintertime? Clim Dyn 41:1835–1852. https://doi.org/10.1007/s00382-012-1570-2

Giannini A, Kushnir Y, Cane MA (2000) Interannual variability of Caribbean rainfall, ENSO, and the Atlantic Ocean. J Clim 13: 297–311. https://doi.org/10.1175/1520-0442(2000)013,0297:IVOCRE.2.0.CO;2

Giannini A, Chiang JCH, Cane MA, Kushnir Y, Seager R (2001) The ENSO teleconnection to the tropical Atlantic Ocean: contributions of the remote and local SSTs to rainfall variability in the tropical Americas. J Clim 14:4530–4544

Graf HF, Zanchettin D (2012) Central Pacific El Niño, the "subtropical bridge," and Eurasian climate. J Geophys Res Atmos 117:D01102. https://doi.org/10.1029/2011JD016493

Ham YG, Kug JS, Park JY, Jin FF (2013) Sea surface temperature in the north tropical Atlantic as a trigger for El Niño/Southern Oscillation events. Nat Geosci 6:112–116. https://doi.org/10.1038/ngeo1686

Ham YG, Sung MK, An SI, Schubert S, Kug JS (2014) Role of tropical Atlantic SST variability as a modulator of El Niño teleconnections. Asia Pac J Atmos Sci 50:247–261. https://doi.org/10.1007/s13143-014-0013-x

Handoh IC, Bigg GR (2000) A self-sustaining climate mode in the tropical Atlantic, 1995–1997: observations and modelling. Q J Roy Meteor Soc 126:807–821

Handoh IC, Matthews AJ, Bigg GR, Steven DP (2006) Interannual variability of tropical Atlantic independent of or associated with ENSO: part 1. The North Tropical Atlantic. Int J Climatol 26:1937–1956. https://doi.org/10.1002/joc.1343

Hatzaki M, Wu RG (2015) The south-eastern Europe winter precipitation variability in relation to the North Atlantic SST. Atmos Res 152:61–68. https://doi.org/10.1016/j.atmosres.2013.10.008

Hegyi BM, Deng Y (2011) A dynamical fingerprint of tropical Pacific sea surface temperatures on the decadal-scale variability of cool-season Arctic precipitation. J Geophys Res 116:D20121. https://doi.org/10.1029/2011JD016001

Hegyi BM, Deng Y, Black RX, Zhou R (2014) Initial transient response of the winter polar stratospheric vortex to idealized equatorial Pacific sea surface temperature anomalies in the NCAR WACCM. J Clim 27:2699–2713. https://doi.org/10.1175/JCLI-D-13-00289.1

Huang B, Shukla J (2005) Ocean-atmosphere interactions in the tropical and subtropical Atlantic Ocean. J Clim 18:1652–1672. https://doi.org/10.1175/JCLI3368.1

Huang JP, Higuchi K, Shabbar A (1998) The relationship between the North Atlantic Oscillation and El Niño-Southern Oscillation. Geophys Res Lett 25:2707–2710. https://doi.org/10.1029/98GL01936

Huang B, Schopf PS, Pan Z (2002) The ENSO effect on the tropical Atlantic variability: a regionally coupled model study. Geophys Res Lett 29:2039. https://doi.org/10.1029/2002GL014872

Huang B, Schopf PS, Shukla J (2004) Intrinsic ocean–atmosphere variability of the tropical Atlantic Ocean. J Clim 17:2058–2077. https://doi.org/10.1175/1520-0442(2004)017,2058:IOVOTT.2.0.CO;2

Huo LW, Guo PW, Hameed SN, Jin DC (2015) The role of tropical Atlantic SST anomalies in modulating western North Pacific tropical cyclone genesis. Geophys Res Lett 42:2378–2384. https://doi.org/10.1002/2015GL063184

Jimenez-Esteve B, Domeisen DIV (2018) The tropospheric pathway of the ENSO-North Atlantic teleconnection. J Clim 31:4563–4584. https://doi.org/10.1175/JCLI-D-17-0716.1

Kalnay E et al (1996) The NCEP/NCAR 40-year reanalysis project. Bull Am Meteor Soc 77:437–471 https://doi.org/10.1175/1520-0477(1996)077,0437:TNYRP.2.0.CO;2

Kao HY, Yu JY (2009) Contrasting eastern-Pacific and central-Pacific types of ENSO. J Clim 22:615–632. https://doi.org/10.1175/2008JCLI2309.1

Klein SA, Soden BJ, Lau NC (1999) Remote sea surface temperature variations during ENSO: evidence for a tropical atmospheric bridge. J Clim 12: 917–932. https://doi.org/10.1175/1520-0442(1999)012%3C0917:RSSTVD%3E2.0.CO;2

Kucharski F, Bracco A, Yoo JH, Tompkins AM, Feudale L, Ruti P, Dell'Aquila A (2009) A Gill-Matsuno-type mechanism explains the tropical Atlantic influence on African and Indian monsoon rainfall. Q J Roy Meteor Soc 135:569–579. https://doi.org/10.1002/qj.406

Kug JS, Jin FF, An SI (2009) Two types of El Niño events: cold tongue El Niño and warm pool El Niño. J Clim 22:1499–1515

Lee SK, Enfield DB, Wang C (2008) Why do some El Niños have no impact on tropical North Atlantic SST? Geophys Res Lett 35:L16705. https://doi.org/10.1029/2008GL034734

Liu Z, Zhang Q, Wu L (2004) Remote impact on tropical Atlantic climate variability: statistical assessment and dynamic assessment. J Clim 17: 1529–1549. https://doi.org/10.1175/1520-0442(2004)017%3C1529:RIOTAC%3E2.0.CO;2

López-Parages J, Rodríguez-Fonseca B, Terray L (2015) A mechanism for the multidecadal modulation of ENSO teleconnection with Europe. Clim Dyn 45:867–880

López-Parages J, Rodríguez-Fonseca B, Dommenget D, Frauen C (2016a) ENSO influence on the North Atlantic European climate: a non-linear and non-stationary approach. Clim Dyn 47:2071–2084

López-Parages J, Rodríguez-Fonseca B, Mohino E, Losada T (2016b) Multidecadal modulation of ENSO teleconnection with Europe in late winter: analysis of CMIP5 models. J Clim 29:8067–8081

Manzini E, Giorgetta MA, Esch M, Kornblueh L, Roeckner E (2006) The influence of sea surface temperatures on the northern winter stratosphere: ensemble simulations with the MAECHAM5 model. J Clim 19:3863–3881

Marshall J, Kushnir Y, Battisti D, Chang P, Czaja A, Dockson R, Hurrell J, McCartney M, Saravanan R, Bisbeck M (2001) North Atlantic climate variability: phenomena, impacts and mechanisms. Int J Climatol 21:1863–1898. https://doi.org/10.1002/joc.693

Martin-Rey M, Rodriguez-Fonseca B, Polo I (2015) Atlantic opportunities for ENSO prediction. Geophys Res Lett 42:6802–6810. https://doi.org/10.1002/2015GL065062

Mo KC, Hakkinen S (2001) Interannual variability in the tropical Atlantic and linkages to the Pacific. J Clim 14:2740–2762

Nobre P, Shukla J (1996) Variations of sea surface temperature, wind stress, and rainfall over the tropical Atlantic and South America. J Clim 9:2464–2479

Perlwitz J, Graf HF (1995) The statistical connection between tropospheric and stratospheric circulation of the Northern Hemisphere in winter. J Clim 8: 2281–2295. https://doi.org/10.1175/1520-0442(1995)008%3C2281:TSCBTA%3E2.0.CO;2

Rayner NA, Parker DE, Horton EB, Folland CK, Alexander LV, Rowell DP, Kent EC, Kaplan A (2003) Global analyses of sea surface temperature, sea ice, and night marine air temperature since the late nineteenth century. J Geophys Res 108:4407. https://doi.org/10.1029/2002JD002670

Rodrigues RR, McPhaden MJ (2014) Why did the 2011–2012 La Niña cause a severe drought in the Brazilian Northeast? Geophys Res Lett 41:1012–1018. https://doi.org/10.1002/2013GL058703

Rodrigues RR, Haarsma RJ, Campos EJD, Ambrizzi T (2011) The impacts of Inter-El Niño variability on the Tropical Atlantic and Northeast Brazil climate. J Clim 24:3402–3422

Saravanan R, Chang P (2000) Interaction between tropical Atlantic variability and El Niño-Southern Oscillation. J Clim 13: 2177–2194. https://doi.org/10.1175/1520-0442(2000)013%3C2177:IBTAVA%3E2.0.CO;2

Smith TM, Reynolds RW, Peterson TC, Lawrimore L (2008) Improvements to NOAA's historical merged land–ocean surface temperature analysis (1880–2006). J Clim 21:2283–2296. https://doi.org/10.1175/2007JCLI2100.1

Sutton RT, Jewson SP, Rowell DP (2000) The elements of climate variability in the tropical Atlantic region. J Clim 13:3261–3284

Takaya K, Nakamura H (2001) A formulation of a phase-independent wave-activity flux for stationary and migratory quasi-geostrophic eddies on a zonally varying basic flow. J Atmos Sci 58(6):608–627. https://doi.org/10.1175/1520-0469(2001)058%3C0608:AFOAPI%3E2.0.CO;2

Taschetto AS, Rodrigues RR, Meehl GA, McGregor S, England MH (2016) How sensitive are the Pacific-North Atlantic teleconnections to the position and intensity of El Niño-related warming. Clim Dyn 46:1841–1860

Wang CZ (2005) ENSO, Atlantic climate variability and the Walker and Hadley circulations. In: Diaz HF, Bradley RS (eds) The Hadley circulation: present, past and future. Cambridge University Press, Cambridge, pp 173–202

Wang X, Wang CZ, Zhou W, Wang DX, Song J (2011) Teleconnected influence of North Atlantic sea surface temperature on the El Niño onset. Clim Dyn 37:663–676. https://doi.org/10.1007/s00382-010-0833-z

Wei K, Takahashi M, Chen W (2015) Long-term changes in the relationship between stratospheric circulation and East Asian winter monsoon. Atmos Sci Let 16:359–365. https://doi.org/10.1002/asl2.568

Weng H, Ashok K, Behera SK, Rao SA, Yamagata T (2007) Impacts of recent El Niño Modoki dry/wet conditions in the Pacific Rim during boreal summer. Clim Dyn 29(2–3):113–129. https://doi.org/10.1007/s00382-007-0234-0

Wu RG, Kirtman BP (2011) Caribbean Sea rainfall variability during the rainy season and relationship to the equatorial Pacific and tropical Atlantic SST. Clim Dyn 37:1533–1550. https://doi.org/10.1007/s00382-010-0927-7

Wu LX, Liu ZY (2002) Is tropical Atlantic variability driven by the North Atlantic Oscillation? Geophys Res Lett 29:1653. https://doi.org/10.1029/2002GL014939

Wu RG, Yang S, Liu S, Sun L, Lian L, Gao ZT (2011) Northeast China summer temperature and North Atlantic SST. J Geophys Res 116:D16116. https://doi.org/10.1029/2011JD015779

Xie SP, Philander SGH (1994) A coupled ocean-atmosphere model of relevance to the ITCZ in the eastern Pacific. Tellus 46A:340–350

Yeh SW, Kug JS, Dewitte B, Kwon MH, Kirkman BP, Jin FF (2009) El Niño in a changing climate. Nature 461:511–514. https://doi.org/10.1038/nature08316

Zhou LT, Wu RG (2015) Interdecadal variability of winter precipitation in NWC and its association with the North Atlantic SST change. Int J Climatol 35:1172–1179. https://doi.org/10.1002/joc.4047